CFD analysis of multiphase blood flow within aorta and its thoracic branches of patient with coarctation of aorta using multiphase Euler - Euler approach

Z Ostrowski[1], B Melka[1], W Adamczyk[1], M Rojczyk[1], A Golda[2] and A J Nowak[1]

[1] Institute of Thermal Technology, Silesian University of Technology, Konarskiego 22, 44-100 Gliwice, Poland
[2] Department of Cardiology, Gliwice Medical Center, Kosciuszki 29, 44-100 Gliwice, Poland

Ziemowit.Ostrowski@polsl.pl

Abstract. In the research a numerical Computational Fluid Dynamics (CFD) model of the pulsatile blood flow was created and analyzed. A real geometry of aorta and its thoracic branches of 8-year old patient diagnosed with a congenital heart defect – coarctation of aorta was used. The inlet boundary condition were implemented as the User Define Function according to measured values of volumetric blood flow. The blood flow was treated as multiphase: plasma, set as the primary fluid phase, was dominant with volume fraction of 0.585 and morphological elements of blood were treated in Euler-Euler approach as dispersed phases (with 90% Red Blood Cells and White Blood Cells as remaining solid volume fraction).

1. Introduction

The untreated coarctation of aorta CoA (narrowing of the descending aorta opposite to the site of the ductus arteriosus insertion) causes premature death of the patients with an average survival of 35 years [1]. The laminar flow in the normal aorta becomes turbulent at the narrowed site and pressure gradient occurs. The negative effect on the cardiovascular system comes from exposure of the upper part of the human body to hypertension and blood flow disturbances with all consequences. Typically, patients with coarctation of aorta suffer from arterial hypertension, coronary artery disease, stroke, endocarditis, heart failure and aortic dissection whereas the organs in the lower part of the body are hypoperfused [2]. According to the American College of Cardiology and American Heart Association guidelines for treatment patients with congenital heart disease indications for the therapeutic intervention in CoA require invasive blood pressure measurement before and after the narrowed site [3]. A non-invasive assessing of the coarctation severity solely on the data from imaging modalities like CT or MRI supported with blood flow modeling using computed fluid dynamics would be very beneficial for the clinical practice.

Modelling of blood flow using Computational Fluid Dynamics (CFD) has recently become more popular and wider available. Development of such computer models opens new perspectives for predicting and solving of many potential problems. CFD technique achieved status of promising tool in bioengineering, where this technique is used for visualization of blood flows within vessels and cavities of the circulatory system. A well validated numerical model for example can suggest solutions how to construct most suitable stents with best deployment within the vessels, visualize blood flow within the artery prior to performing a percutaneous coronary intervention and estimate the significance of vascular

lesions [1]. Nonetheless, except of many advantages, the CFD methods are still not ready for clinical use. This is mainly caused by time demanding simulations due to very unstable flow phenomena which require using of complex unsteady solvers.

The most common approach used during modelling of the blood flow is a single phase simplification of the blood rheological character. In this approach properties of blood are represented by average density and viscosity for plasma and morphotic elements with vessels represented by rigid walls [2] - [3]. In literature some numerical models describe flow within a selected section of the human circulatory system and an additionally implement a coupled lumped model for simulations of both – a part and a whole cardiovascular system [4] - [6]. For the CFD simulations it is crucial to establish a precise geometry of the flow field. The geometric data for the aorta is typically obtained from the Computed Tomography (CT) or Magnetic Resonance Imaging (MRI) scans. The preparation of geometric data for numerical simulations is an important task and requires special attention [7].

There are other mathematical models which can be used for modelling blood flow, for example multifluid techniques like Euler-Euler (EE) or hybrid Euler-Lagrange (EL). The multiphase approach is used less frequently than single phase models. For the multiphase blood modelling with Euler-Euler technique, plasma and morphological elements are treated as continuous and interpenetrating phases. The EE approach is typically used for modelling narrow vessels where Fahraeus–Lindqvist effect occurs [8] - [10]. The current publication presents an utilization of a three-fluid Euler-Euler approach for modelling of blood flow within the aorta and its main thoracic branches of a 8-year-old patient suffering from coarctation of aorta (flow through the coronary arteries was omitted).

2. Geometrical model

The geometry of the aorta was rendered from patients data acquired using Gadolinium-enhanced Magnetic Resonance Angiography (MRA). The numerical case was based on geometry and data defined in CFD challenge problem for development numerical models capable to model blood flow (OSMSC Corp., USA) [11]. The investigated geometry after conversion to solid model using GeomagicDesignX (3D Systems, Inc., USA) software is shown in Figure 1. In numerical simulation, the walls of the domain were treated as rigid one.

The generated mesh consists of about 700,000 of hybrid elements. In the inlet part mostly hexahedral elements were used in order to stabilize flow and accurately prescribe velocity profile.

At the inlet the velocity boundary conditions was used. For all outlets the outflow condition was used, where the flow rate was controlled by weight factor taken from [11].

3. Numerical model

The crucial point in modelling of blood flow is to accurately define the boundary condition at the inlet to the computational domain. In presented work the velocity inlet, based on the volumetric flow profile, has been set to mimic the conditions during the human cardiac cycle. Whole cycle has been divided into 20 points (with linear interpolation between them), where volumetric flow values were taken from a phase-contrast (PC) MRI through-plane velocity encoding [11]. The pulsatile and repeated boundary condition was implemented into the solution procedure by the set of User Define Functions (UDFs). The volumetric flow profiles for specific blood phases are depicted in Figure 2. The hematocrit of 0.405 (vol.) was used in numerical simulations which is a value within the normal range. Two vertical red lines in Figure 2 represent characteristic moments of the cardiac cycle (systole and diastole). All results in the paper are discussed for these two specific points of time.

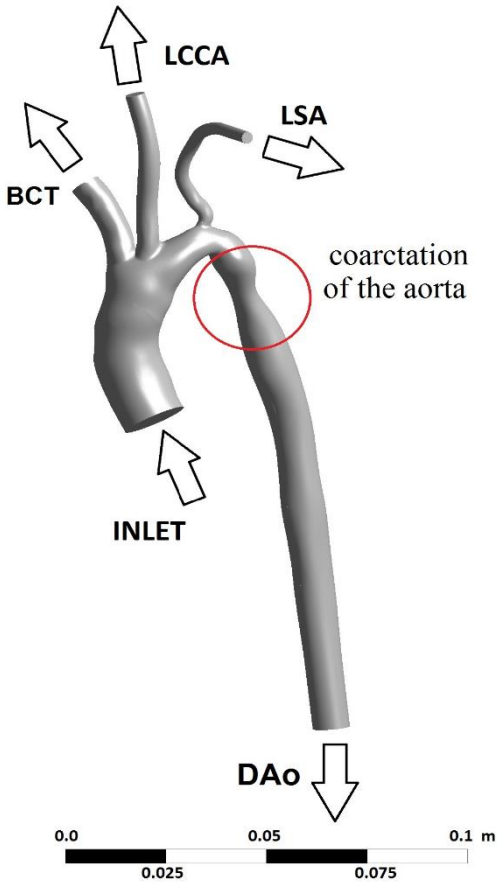

Figure 1. The geometry of blood volume in coarcted aorta and its thoracic branches used in CFD model,

BCT: flow through brachiocephalic trunk;
LCCA: flow through left common carotid artery;
LSA: flow through left subclavian artery;
DAo: flow through descending aorta.

Volumetric share of blood flow on the outflows, based on [11] were implemented in the model as outflow boundary condition (cf. Table 1). Description of the shortcuts used in the table is pointed out in Figure 1 caption.

The characteristic parameters used in the numerical model definition are presented in Table 2. It contains material properties of specific phases and the coefficients describing walls behavior.

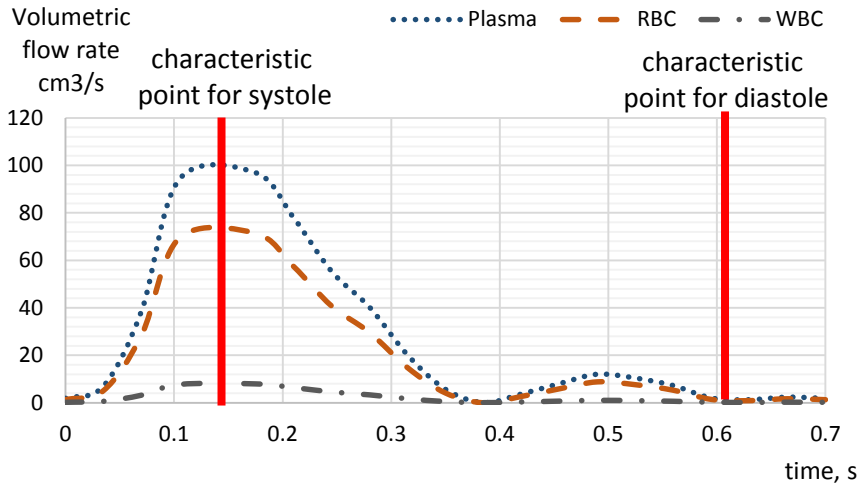

Figure 2. Volumetric flow at the inlet with share of the specific phases

Table 1. The volumetric outflow share of blood flow on the artery branches

Outflow	BT	LCCA	LSA	DAo
% Ascending Aortic Flow	25.6	11.3	4.3	58.8

The volume fraction of fluid and solid phases sums up to 1 according to eq. (1).

$$\varepsilon_f + \varepsilon_{WBC} + \varepsilon_{RBC} = 1 \tag{1}$$

The principle of mass conservation in the multiphase flow is described by Eq. (2) for the fluid phase, i.e. Plasma with subscript *f* and by Eq. (3) for solid phases, where subscript *s* represents RBC and WBC phases respectively. In current research, neither mechanism of mass exchange between specific phases nor any mass sources are considered, yielding the right side of continuity equations being zero.

$$\frac{\partial(\rho_f \varepsilon_f)}{\partial t} + \nabla \cdot \left(\rho_f \varepsilon_f \overrightarrow{v_f}\right) = 0 \tag{2}$$

$$\frac{\partial(\rho_s \varepsilon_s)}{\partial t} + \nabla \cdot (\rho_s \varepsilon_s \overrightarrow{v_s}) = 0 \tag{3}$$

The principle of momentum conservation in the multiphase flow can be written for the fluid phase as in Eq. (4). To calculate momentum for the solid phases, (5) is applied twice for the RBC and WBC separately.

$$\frac{\partial\left(\rho_f \varepsilon_f \overrightarrow{v_f}\right)}{\partial t} + \nabla \cdot \left(\rho_f \varepsilon_f \overrightarrow{v_f}\overrightarrow{v_f}\right) = \rho_f \varepsilon_f \vec{g} - \varepsilon_f \nabla P + \nabla \cdot \overrightarrow{\overrightarrow{\tau_f}} + \sum_{s=1}^{N_s} (K_{sf}(\overrightarrow{v_s} - \overrightarrow{v_f})) \tag{4}$$

$$\frac{\partial(\rho_s \varepsilon_s \overrightarrow{v_s})}{\partial t} + \nabla \cdot (\rho_s \varepsilon_s \overrightarrow{v_s}\overrightarrow{v_s}) = \rho_s \varepsilon_s \vec{g} - \varepsilon_s \nabla P - \nabla P_s + \nabla \cdot \overrightarrow{\overrightarrow{\tau_s}} + K_{fs}(\overrightarrow{v_f} - \overrightarrow{v_s}) + \sum_{q}^{N_s - 1} (K_{qs}(\overrightarrow{v_q} - \overrightarrow{v_s})) \tag{5}$$

Subscript *s* represents RBC and WBC solid phase respectively. Subscript *q* is RBC or WBC depending on configuration (while $q \neq s$), N_s expresses the number of solid phases (here N_s=2). *P* represents pressure of fluid and P_s is a granular pressure. The $\vec{g}$ is gravitational acceleration, $\vec{\tau}$ is stress tensor and *K* is the interphase exchange momentum coefficient.

Granular temperature parameter used in the kinetic theory is associated with the random motion of particles or, in other words, particle velocity fluctuations. It is a component needed for the calculation of random kinetic energy of solid phases according to (6) based on [8], [12]. This value, depicted as θ_s, is used to calculate closure terms, for instance, granular pressure (collision, kinetic and friction), granular viscosity (collision, kinetic and friction), and solid stress tensor. The diffusion coefficient for granular energy k_{θ_s} can be expressed by (7). Where η is presented by using (8).

$$\frac{\partial}{\partial t}(\rho_s \varepsilon_s \theta_s) + \nabla \cdot (\rho_s \varepsilon_s \overrightarrow{v_s} \theta_s) = (-p_s + \bar{I}\tau_s) : \nabla \overrightarrow{v_s} + \nabla \cdot \left(k_{\theta_s} \nabla \theta_s\right) - \frac{12(1 - {e_{ss}}^2) g_{0,ss}}{d_s \sqrt{\pi}} \rho_s {\varepsilon_s}^2 {\theta_s}^{\frac{3}{2}} \tag{6}$$

$$k_{\theta_s} = \frac{15 d_s \rho_s \varepsilon_s \sqrt{\theta_s \pi}}{4(41 - 33\eta)} \left[1 + \frac{12}{5}\eta^2 (4\eta - 3)\varepsilon_s g_{0,ss} + \frac{16}{15\pi}(41 - 33\eta)\eta \varepsilon_s g_{0,ss}\right] \tag{7}$$

$$\eta = \frac{1}{2}(1 + e_{ss}) \tag{8}$$

To solve interaction between phases, influence of RBC and WBC presence on plasma flow a number of closure terms in equations (4), (5), (6), (7) and (8) have to be defined. The detailed description of the closures terms responsible for modeling granular pressure, granular and bulk viscosities, etc. can be found in [14] - [16].

The momentum exchange coefficients (*K)* between plasma and RBC treating as a dense granular flow were calculated applying Gidaspow [14] drag model. Whereas, the WBC was treated as the dilute granular phase, so Wen&Yu drag model [17] was sufficient to predict interphase momentum exchange.

Table 2. Characteristic parameters assumed in simulation

Plasma density, $kg \cdot m^{-3}$	1020
RBC density, $kg \cdot m^{-3}$	1080
WBC density, $kg \cdot m^{-3}$	1080
Plasma viscosity $kg \cdot m^{-1} \cdot s^{-1}$	0.0035
inlet RBC volumetric fraction	0.405
inlet WBC volumetric fraction	0.01
Restitution coefficient	0.9999
Wall restitution coefficient	0.9999
Time step, s	0.005

The interaction between granular/dispersed phases (RBC-WBC) were calculated using symmetrical drag model [18].

The turbulence effect was taken into account by selecting the standard k-ε model, where the kinetic (k) and dissipation (ε) of energy were calculated per each phase [19]. Model was adequate for current mesh resolution and model configuration. The restitution coefficient (e), shown in the Table 2, is the parameter of the mathematical model that describes interactions/collision of RBC and WBC with walls and between each other. This value is close to 1 while kinetic energy between WBC and RBC before and after their collision almost did not change.

4. Results

Presented relative static pressures are referred to the pressure on the descending thoracic aorta domain outlet. The pressure field on the domain walls for the characteristic point during systole is presented in Figure 3. The highest pressures of about 5 kPa occurred in the region of inlet. During the systole, the smallest static pressure can be noticed in the aortic coarctation and its relative pressure reached -5.7 kPa. Thus, the maximum pressure difference in the computational domain for the systole was on the level of 11 kPa.

According to the pressure field, presented in Figure 4, for the diastole characteristic point the maximum pressure difference reaches 40 Pa. In this case, the highest pressure was at the outlet of descending aorta and was also referred to its whole field. The lowest pressure for the diastole was on the main inlet and before coarctation severity. The static pressure level was significantly smaller in comparison with the systole.

Wall shear stress caused by the plasma phase flow on the rigid walls of the blood vessel was the highest before the CoA. It reached 227 Pa and was located on the opposite wall to the left subclavian artery bifurcation in the case of systole (pointed in Figure 5).

According to Figure 5, the wall shear stress caused by the plasma on the descending aorta narrowed site was on the level of 100 Pa. During diastole, the maximum wall shear stress caused by plasma phase was reduced of about 1.5 Pa and was located also before aorta coarctation region. Figure 6 illustrates only the wall shear stress during diastole.

The velocity vectors in the bifurcation region of BT, LCCA and LSA from the main aorta is shown in Figure 7 during systole. To clarify the flow field view the velocity was scaled to 2 m/s. The highest velocity values occurred in the CoA and reached over 4 m/s. It influenced directly the high wall shear stress presented in Figure 5. Based on the velocity field analysis, it can be deduced that during systole, the flow was stable without reversed flows at the outflows boundary conditions. From the inlet, blood flowed to the specific outflows according to set boundary conditions. The simulated flow looked mostly laminar. Some eddies occurred in aorta distally to the point where the left subclavian artery comes off

and proximally to the coarctation of aorta. The smallest velocity values were present in the close vicinity of the blood vessel walls.

During diastole the volumetric flow was nearly zero. The pressure gradient was reversed in comparison to the systole (as shown earlier). The reversed flow occurred on each outflow as seen from the numerical simulation. The velocity field for this specific time was illustrated by the velocity vectors in Figure 7. The highest velocities occurred before coarctation of aorta and reached 0.15 m/s. This maximum velocity is 28 times smaller than during systole. The velocity filed analysis can indicate that flow was chaotic and irregular during diastole. In the presented area, numerous eddies are visible.

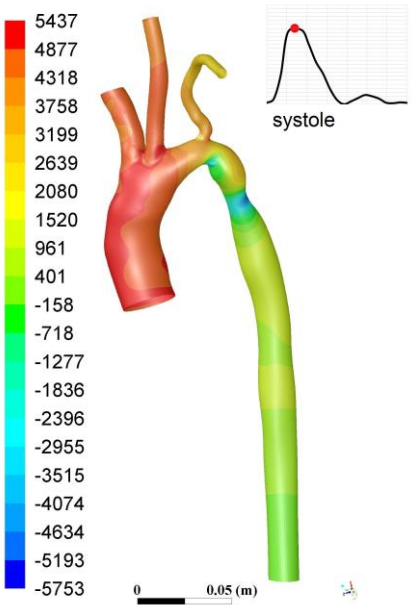

Figure 3. Pressure field in Pa on the walls during systole

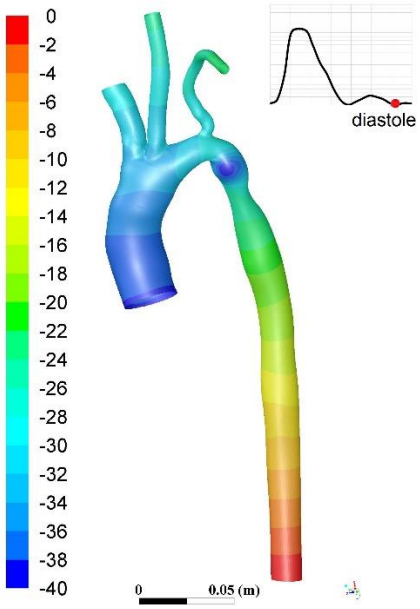

Figure 4. Pressure field in Pa on the walls during diastole

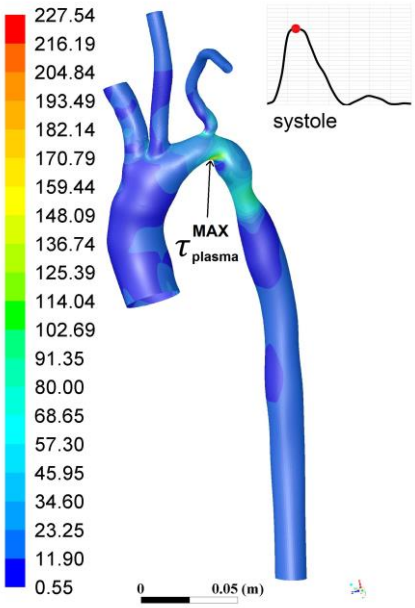

Figure 5. Wall shear stress in Pa during systole

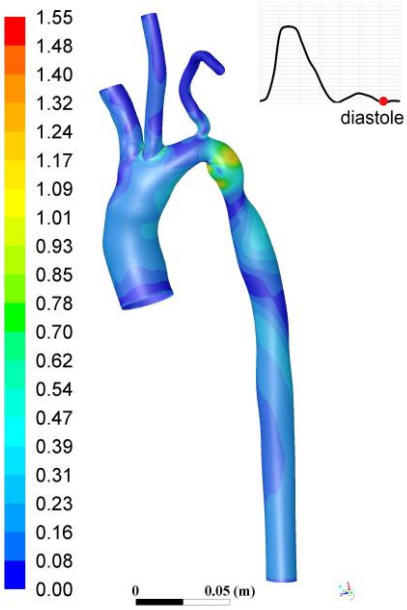

Figure 6. Wall shear stress in Pa during diastole

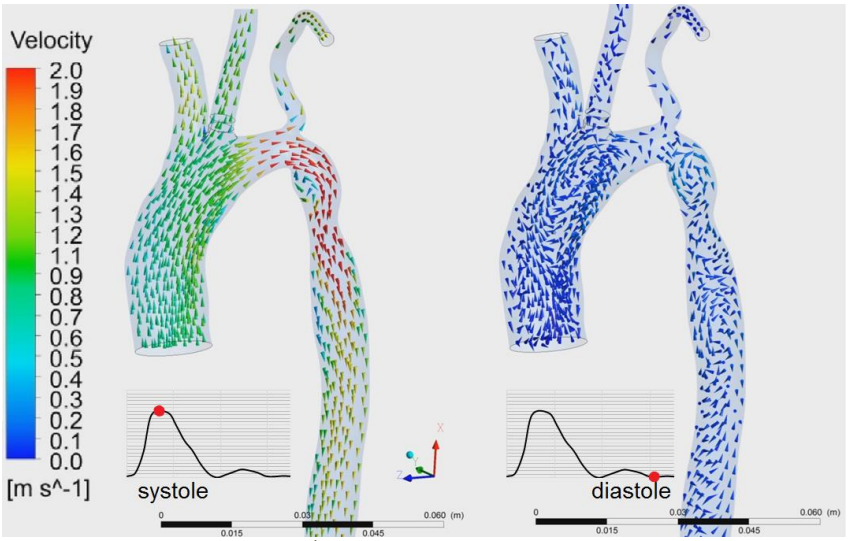

Figure 7. Velocity vectors in $m \cdot s^{-1}$ during systole (left) and during diastole (right).

The volumetric fraction field of phase which was the greatest fraction beyond plasma was presented in Figure 8. The simulation results in cross section of ascending and descending aorta was shown.

The smallest-values of the RBC volume fraction dominated in cross-section area starting from walls are presented in the plane of coarctation region. Migration of RBC from the walls to the center direction could be caused by rising granular temperature in the walls vicinity according to multiphase kinetic theory [10]. The maximum values of granular temperature occurred in some distance from the walls. The maximum values of RBC fraction for the cross section of descending aorta are of 0.406.

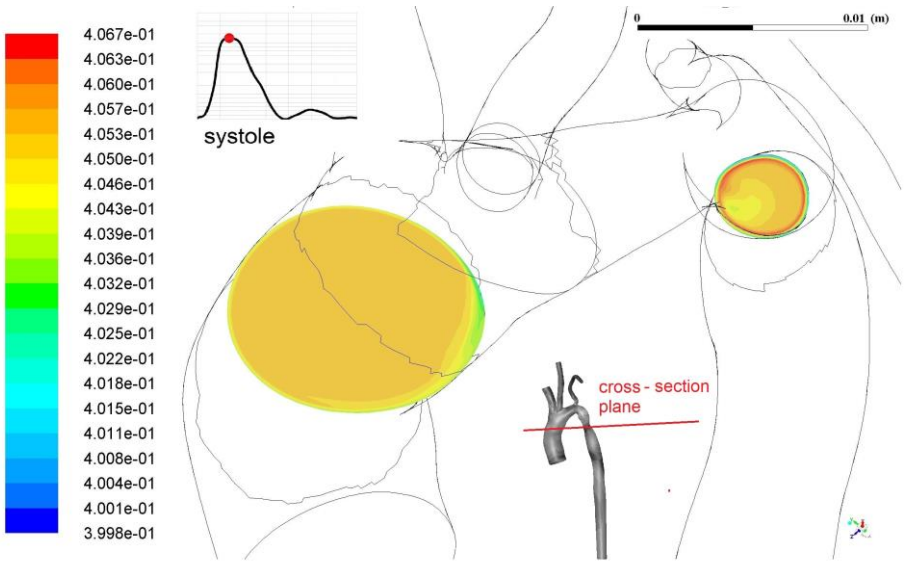

Figure 8. Volumetric fraction of the RBC phase expressed in cross sections of ascending aorta (left) and descending aorta narrowing (right) during systole

5. Conclusions

The scope of the present study was to show an application of computer model for modelling blood flow within aorta and its major thoracic branches of 8-year old patient diagnosed with a congenital heart defect - coarctation of the aorta (CoA, approx. 65% aortic area reduction). Two main types of morphological elements - RBCs and WBCs were represented by two separate granular phases modelled in the Euler - Euler approach, while the primary phase was plasma. The fields of pressure, wall share stress,

velocity and volume fractions were presented for the two characteristic points of the heart cycle (during systole and diastole).

Acknowledgements
This research is supported by National Science Centre (Poland) within projects No 2014/13/B/ST8/04225 and No 2014/15/D/ST8/02620 (for making GeoMagic Design X software available to the research team). This help is gratefully acknowledged herewith.

References

[1] Mortier P, Wentzel J, De Santis G, Chiastra C, Migliavacca F, De Beule M, Louvard Y and Dubini G 2015 Patient-specific computer modelling of coronary bifurcation stenting: the John Doe programme *EuroIntervention* **11(**5) V35-9
[2] Oshima M, Torii R and Kobayashi T 2001 Finite element simulation of blood flow in the cerebral artery *Comp. Meth. Appl. Mech. Eng.* **191**(6–7) 661–71
[3] Long Q, Xu X Yun, Ariff B, Thom S, Hughes A and Stanton A 2000 Reconstruction of Blood Flow Patterns in a Human Carotid Bifurcation : A Combined CFD and MRI Study *J. Magn. Reson. Im.* **11** 299–311
[4] Gharahi H, Zambrano B, Zhu D, DeMarco K and Baek S 2016 Computational fluid dynamic simulation of human carotid artery bifurcation based on anatomy and volumetric blood flow rate measured with magnetic resonance imaging *Int. J. Adv. Eng. Sci. Appl. Math.* **8** 46-60
[5] Traeger B, Srivatsa S, Beussman K, Wang Y, Suzen Y,·Rybicki F, Mazur W, Miszalski-Jamka T 2016 Methodological inaccuracies in clinical aortic valve severity assessment: insights from computational fluid dynamic modeling of CT-derived aortic valve anatomy *Theor. Comput. Fl. Dyn.* **30** 107–28
[6] DeCampli, W, Argueta-Morales R, Divo E and Kassab A 2012 Computational fluid dynamics in congenital heart disease *Cardiol. Young* **22**(6) 800-8
[7] Prince M, Narasimham D, Jacoby W, Williams D, Cho K, Marx M and Deeb G 1996 Three-dimensional gadolinium-enhanced MR angiography of the thoracic aorta *AJR* **166**(6) 1387-97
[8] Gidaspow D, Huang J 2009 Kinetic theory based model for blood flow and its viscosity *Ann. Biomed. Eng.* **37** 1534-45
[9] Huang J, Lyczkowski R and Gidaspow D 2009 Pulsatile flow in a coronary artery using multiphase kinetic theory *J. Biomech.* **42** 743-54
[10] Gidaspown D and Chandra V 2014 Unequal granular temperature model for motion of platelets to the wall and red blood cells to the center *Chem. Eng. Sci.* **117** 107–13
[11] CFD Challenge problem: http://www.vascularmodel.org/miccai2012 (accessed Jan 2016)
[12] Ding J and Gidaspow D 1990 A Bubbling Fluidization Model Using Kinetic Theory of Granular Flow *AIChE J.* **36**(4) 523–38
[13] ANSYS® Academic Research, Release 16.2, ANSYS, Inc.
[14] Gidaspow D 1994 *Multiphase Flow and Fluidization: Continuum and Kinetic Theory Description*s (New York: Academic Press)
[15] Adamczyk W P, Węcel G, Klajny M, Kozołub P, Klimanek A, Białecki R A 2014 Modeling of particle transport and combustion phenomena in a large-scale circulating fluidized bed boiler using a hybrid Euler–Lagrange approach *Particuology* **16** 29-40
[16] Adamczyk W A, Kozołub P, Węcel G, Kliamenk A, Białecki R A, Czakiert T 2014 Modeling oxy-fuel combustion in a 3D circulating fluidized bed using the hybrid Eulere-Lagrange approach *Applied Thermal Engineering* **71** 266-275,
[17] Wen C and Yu Y 1966 Mechanics of fluidization *Chem. Eng. Prog. Symp* **62** 100–11
[18] Syamlal M 1987 *The Particle-Particle Drag Term in a Multiparticle Model of Fluidization* (National Technical Information Service, Springfield)
[19] Anderson J 1995 *Computational fluid dynamics. The basics with applications* (McGraw-Hill, New York)